Supporting Information

Phosphate Ions Reverse the Phase Composition of Silk Fibroin Condensates

*Martin Zaki, Heena Faulder, Rangam Rajkhowa, Matthew McKenzie, Joselito Macabuhay Razal, Dylan Yalmar Hegh, Chris Holland, Benjamin J. Allardyce**

Additional data comparing natural LLPS and phosphate-induced LLPS

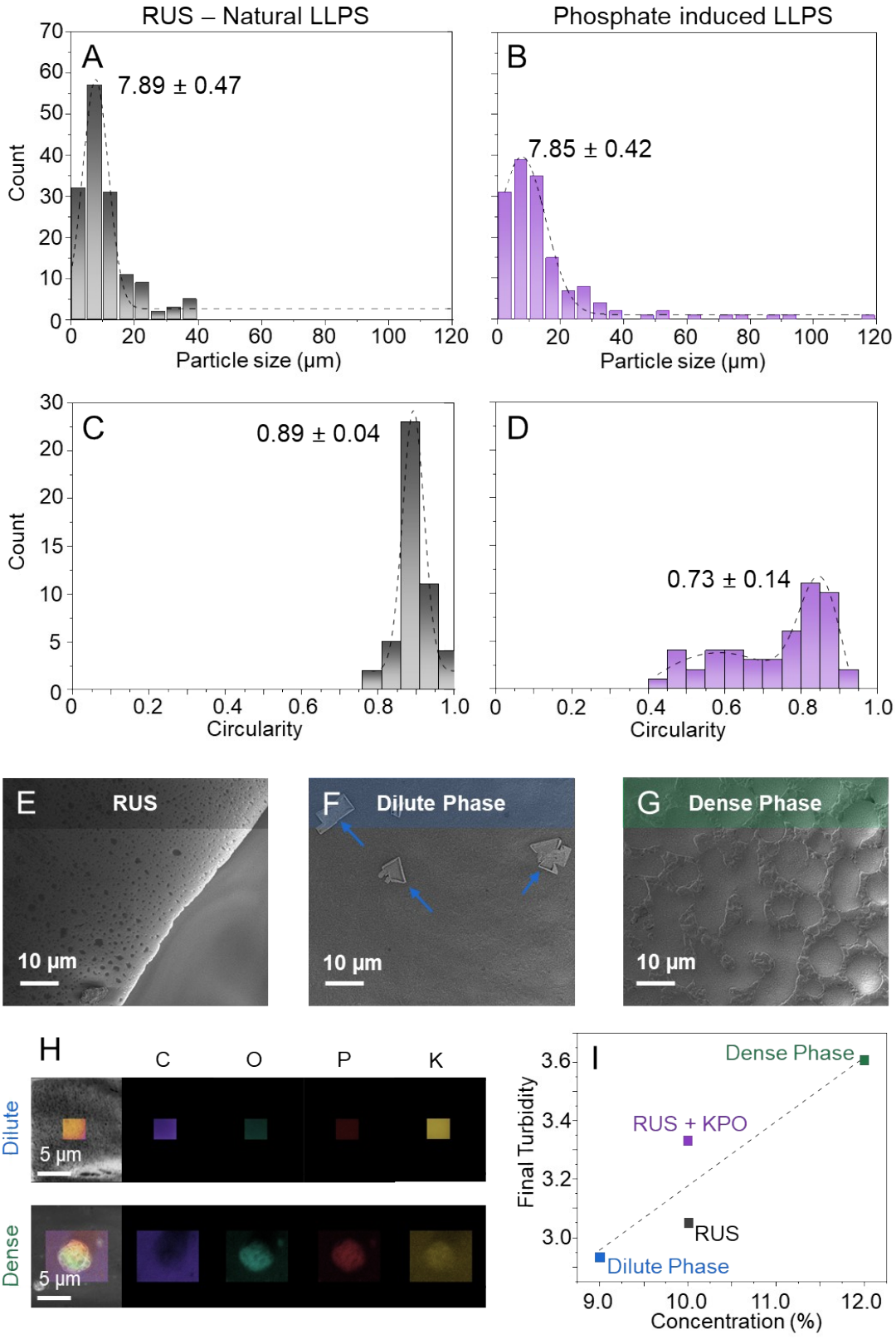

Figure S1. Supporting data comparing natural LLPS and phosphate-induced LLPS. A and B) particle size distribution of the condensates, where the reported values are mode average ±

Standard deviation. Sample size is n=150. Although the average diameters are similar, the polydispersity is greater with potassium phosphate, with some condensates reaching 120 μm. C and D) circularity of the droplets measured using ImageJ. Sample size is n=50. EsB-SEM images at lower magnification of dried RUS films obtained from the gradual evaporation of sessile droplets. E) RUS without phosphate produces dries into a continuous film, with dark droplets within a light matrix. F) Likewise, the dilute phase dries into a continuous film, but residual phosphate is visible (arrows). G) The dense phase dries into a film with distinct phase separation. H) SEM images used to obtain EDS spectra, and the elemental mapping of C, O, P, K for the dilute and dense phases. I) Final turbidity of gelation stability tests as a function of concentration, with a difference of approximately 1 absorbance unit between the dilute and dense phases. In general, increase in concentration leads to an increase in final turbidity, however, it is likely that salts would contribute to turbidity measurements. The contribution from the salt is likely responsible for the observed difference between RUS with and without phosphate.

Table S1. Elemental composition (%) of C, N, O, P, K for the dilute and dense phases obtained from EDS spectra in Figure S1H.

	Elemental composition (%)	
Element Name	**Dilute Phase**	**Dense Phase - condensate**
Carbon	60.14	43.90
Nitrogen	14.75	11.43
Oxygen	21.78	34.27
Phosphorous	0.27	3.49
Potassium	3.06	6.91

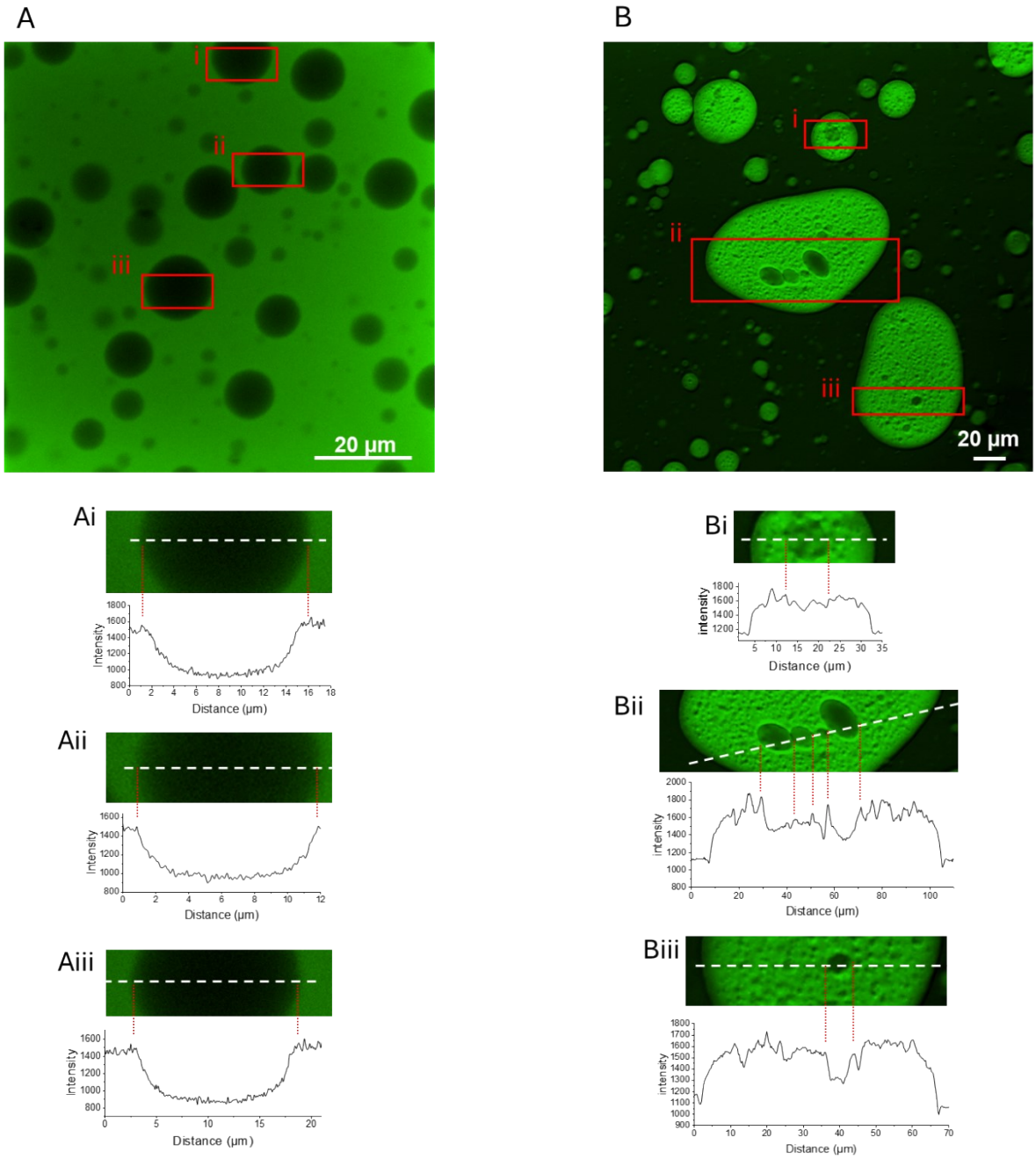

Figure S2. Fluorescence intensity plot profiles of A) salt-free RUS exhibiting natural LLPS and B) 200mM phosphate-induced LLPS.

Identifying the phase boundaries of LLPS

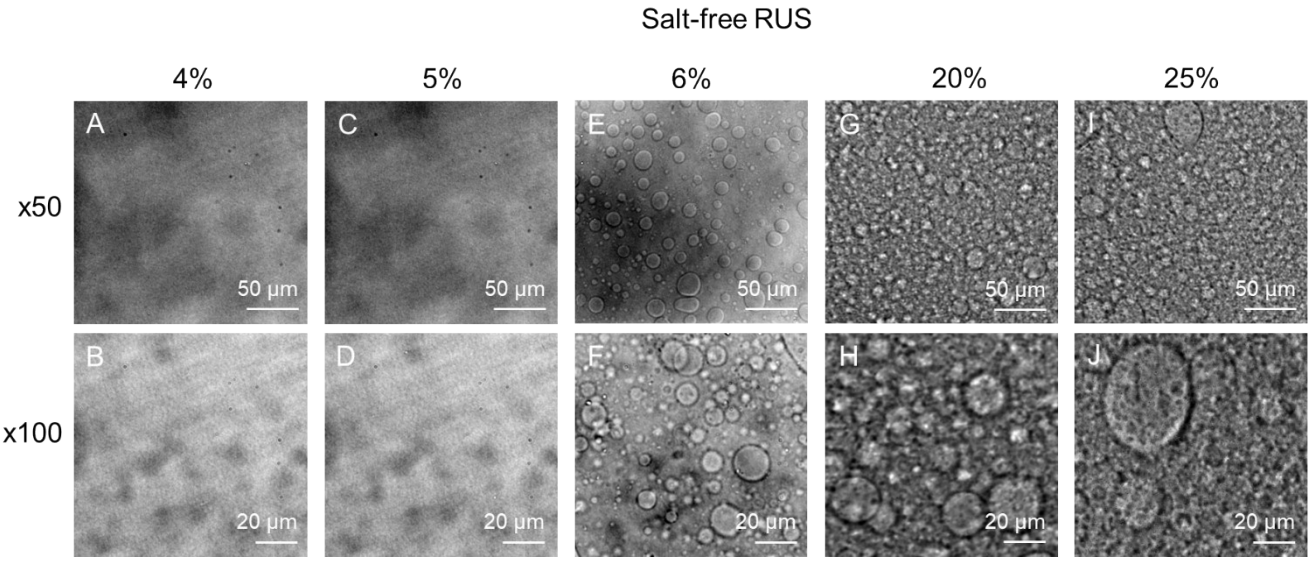

Figure S3. Optical images at x50 and x100 magnifications of 20mM KPO: 1 % RUS solutions at different concentrations. No condensates are visible in 4 % (A and B) and 5 % (C and D), however increasing the concentration to 6 % (D and E) leads to the formation of LLPS, indicating that the threshold for natural LLPS formation occurs between 5 and 6 %. Natural LLPS is present at higher concentrations including 20 % and 25 %, however it was not possible to obtain solutions above 25 % due to silks instability at high concentrations.

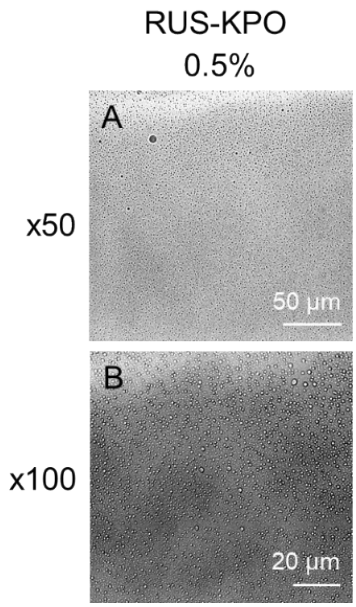

Figure S4. Optical images at A) x50 and B) x100 magnifications of RUS-KPO solution at 0.5 % and 10mM KPO. Small condensates were present in RUS-KPO solutions in concentrations as low as 0.5 % more than 10x lower than the threshold for natural LLPS formation, highlighting that phosphate has a significant influence in altering LLPS assembly.

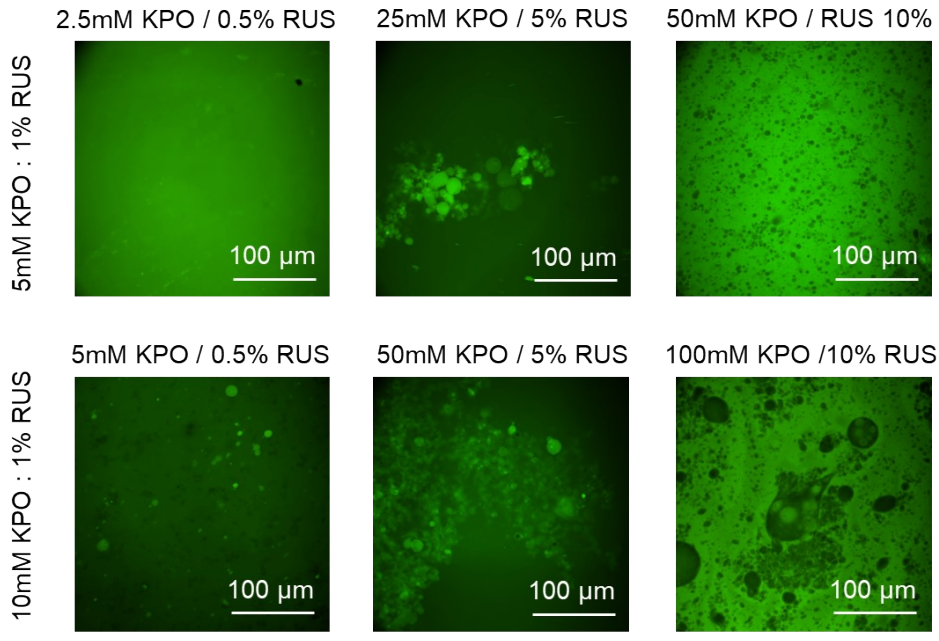

Figure S5. Supplementary confocal fluorescence images of RUS solutions across a range of phosphate (mM) and protein (%) concentrations. No phase separation was observed at 2.5 mM phosphate and 0.5% RUS. In contrast, fluorescent condensates formed at 5 mM/0.5 %, 25

mM/5 %, and 50 mM/5 %, while 50 mM/10 % produced dark condensates within a fluorescent continuous phase. Notably, at 100 mM/10 %, multiple distinct phases emerged, suggesting a compositional threshold at which dark condensates transition to fluorescent condensates.

Gradual evaporation of sessile drops

To understand how concentration alters as the solution droplets dry, the mass was recorded during drying, and the concentration was calculated using the final dry weight (**Figure S6)**. RUS samples with and without phosphate exhibited markedly different drying behaviors. The phosphate-containing RUS dried more rapidly, completing the process in 35 minutes, whereas the salt-free RUS dried more gradually, taking up to 42 minutes to fully evaporate. This effect is likely due to phosphate altering the chemical potential of the water and thus its affinity for silk,[1, 2] thereby enhancing drying. Interestingly, when phosphate at the same concentration but without silk was compared to water alone, it dried slightly more slowly. This suggests that the faster drying observed for RUS with phosphate arises from specific interactions between the salt and silk, rather than from the salt alone. However, drying creates a concentration gradient across the droplet, with differences between the perimeter and the center. Consequently, these mass measurements capture the bulk concentration and overlook specific concentrations at various regions of the droplet. To account for the complexity of the drying kinetics (surface area, contact angles, salts), we try to compare the bulk concentration–time profile with fluorescent images obtained at the droplet edge over time (**Figure S7, S8)**.

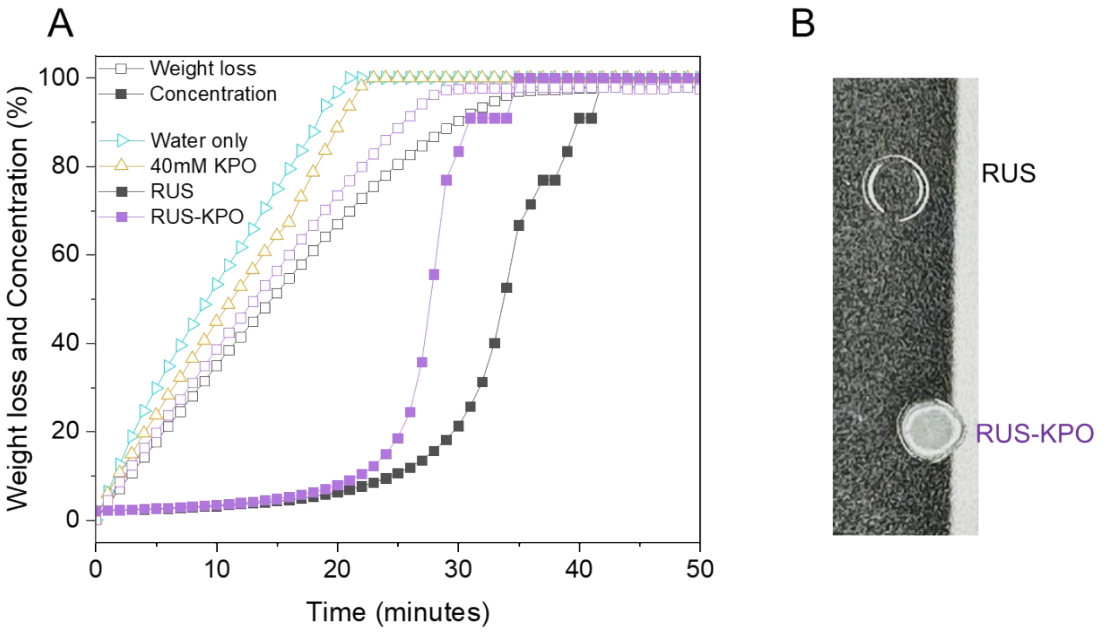

Figure S6. A) Weight loss and concentration of 5 µL droplets drying over time. The concentration was calculated using the final weight of the film. B) Top-down image of dried RUS solutions.

When fluorescent microscopy was used to image the drying of 2 % RUS droplets, natural LLPS formation started to be observed at 1 minute (**Figure S7, Video S1**). Importantly, the condensates remained dark and did not recruit the fluorescent protein throughout drying, indicating that phosphate interactions alter the fundamental nature of protein LLPS formation. Additionally, over time the fluorescent protein was observed to accumulate at the droplet perimeter. However, during the gradual evaporation experiment, the bulk concentrations of salt-free RUS at the time points where LLPS was observed remained below the known bulk concentration threshold for LLPS formation, indicating that these bulk values do not accurately reflect the true local concentrations. Together with the protein accumulation at the perimeter, this made it clear that LLPS was driven by local concentration effects and therefore it was not

possible to definitively determine how high concentrations (>25 %) alter the phase diagram for salt-free RUS.

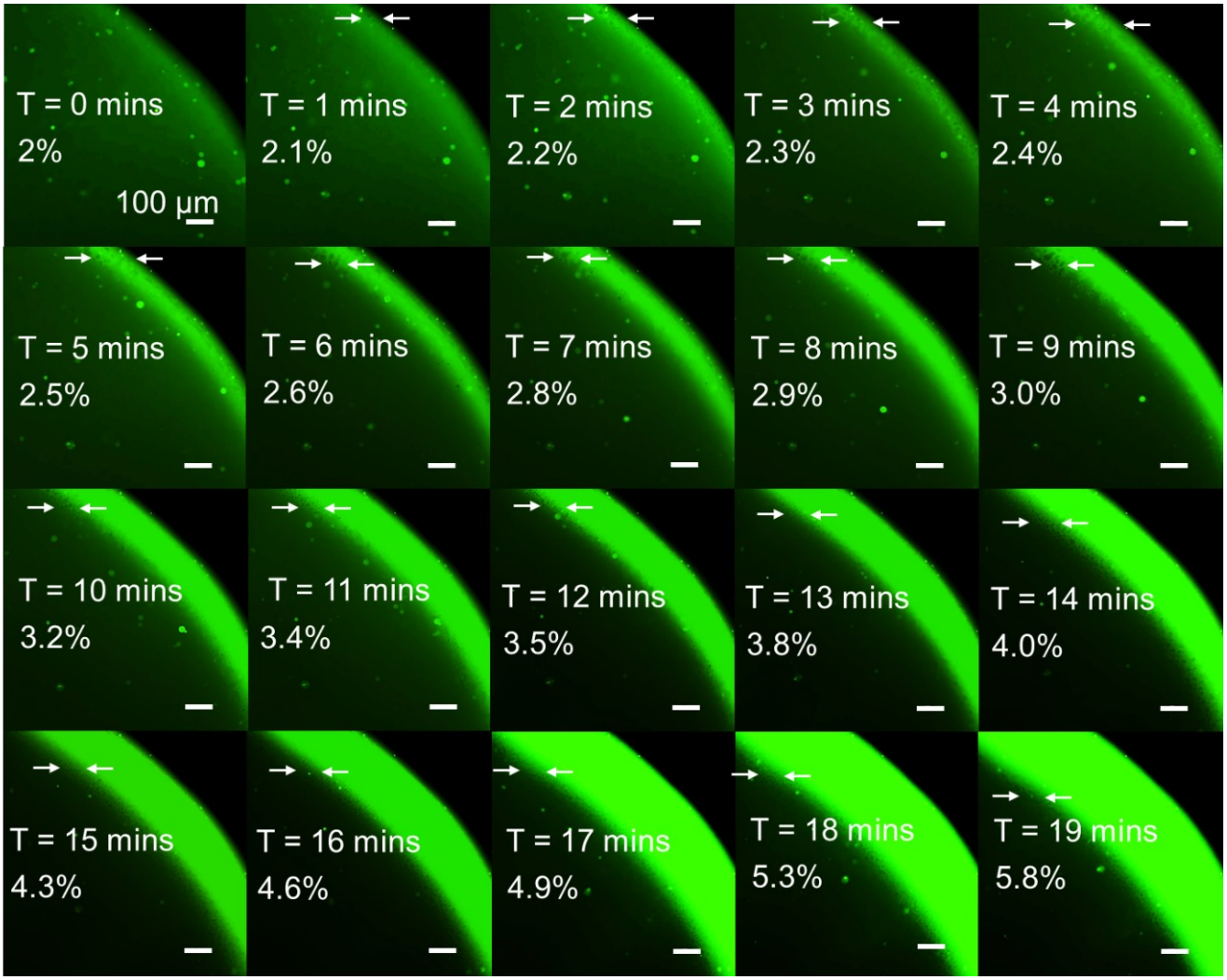

Figure S7. Fluorescent microscopy images of the gradual evaporation of 5 μL 2 % RUS (no salts) drop on a glass slide, alongside measurements of the bulk concentration during drying obtained from Figure S4. As the solution dries, LLPS starts to develop (white arrows). Since the perimeter concentrates more rapidly than the center, the bulk concentration likely underestimates the true local concentration at the droplet edge.

Like the salt-free solution, RUS-KPO had a growing fluorescent perimeter as the solution dried (**Figure S8, Video S2**). However, contrary to salt-free RUS, which had dark condensates, RUS-KPO condensates were fluorescent and present throughout drying. As the condensates of both salt-free RUS and RUS-KPO remained either respectively non-fluorescent or fluorescent throughout drying, this suggests that phosphate interactions fundamentally alter the nature of protein LLPS formation and that the fluorescent protein is not recruited into condensates as a function of concentration.

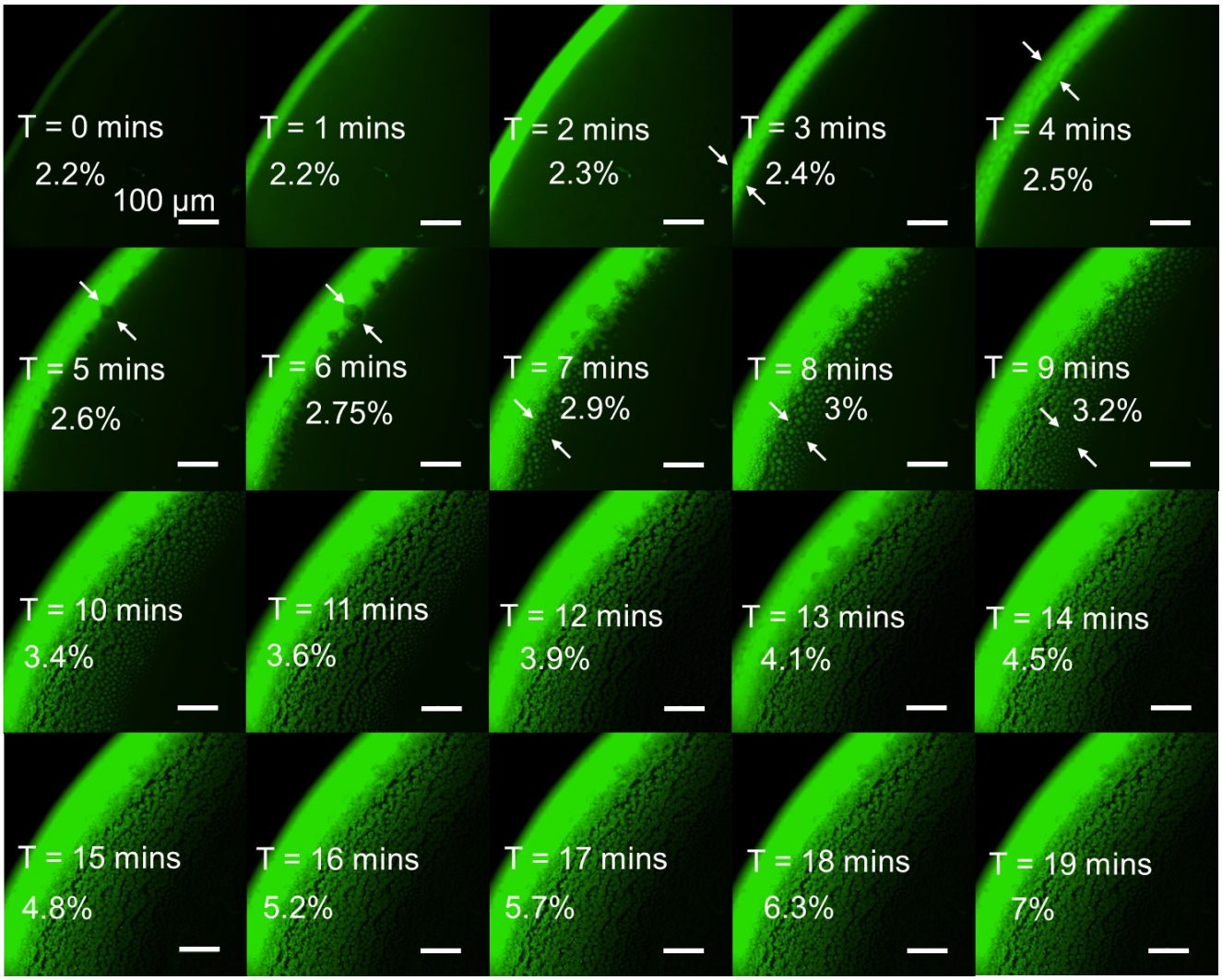

Figure S8. Fluorescent microscopy images of the gradual evaporation of 5 µL 2 % RUS-KPO drop on a glass slide, alongside measurements of the bulk concentration during drying. As the solution dries, fluorescent condensates develop (white arrows), which retain their structure after complete drying.

Protein localization

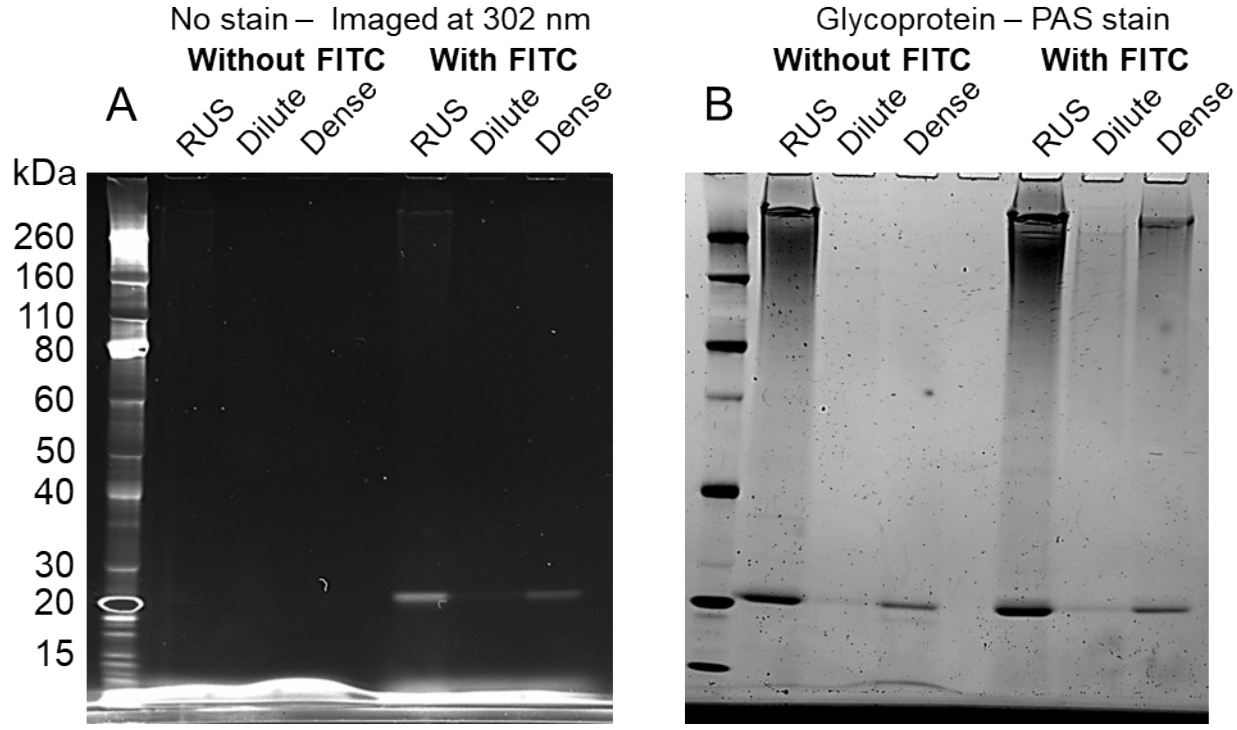

Figure S9. 4-12 % gel of RUS solutions with and without FITC imaged under A) UV light and subsequently with B) visible light after glycoprotein-PAS staining. Glycoprotein staining revealed that FITC preferentially binds to glycoproteins in the silk solution, and PAS stain may co-localize with FITC-labelled proteins. Therefore, PAS staining should be avoided when proteins are pre-labelled with FITC, since the overlap in signals prevents definite identification of glycoproteins.

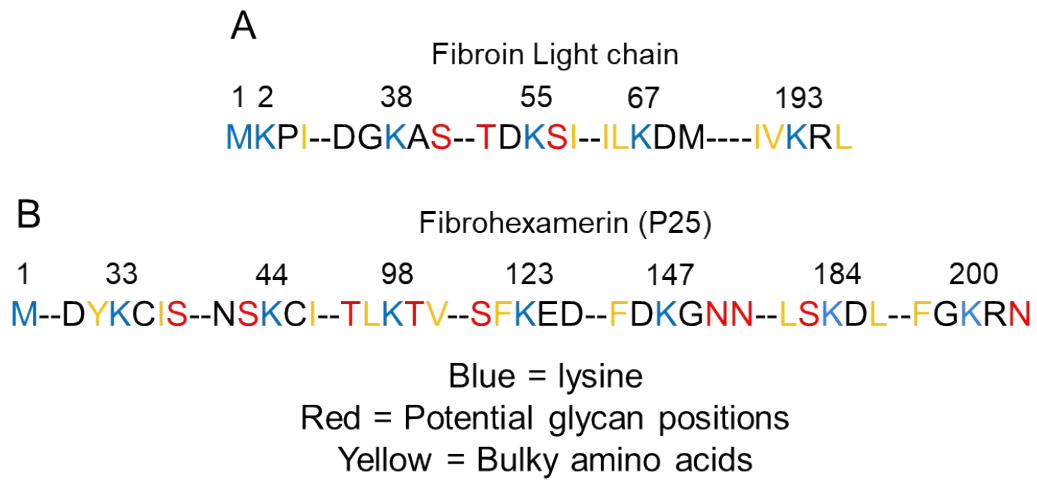

Figure S10. Simplified amino acid sequences of the A) the Fibroin light chain and B) Fibrohexamerin proteins illustrating steric hindrance around lysine (K) residues. The model assumes the presence of glycans at all asparagine (N-linked) and serine/threonine (O-linked) sites in both proteins, although glycosylation has not been experimentally confirmed for the light chain. Bulky amino acids contributing to additional steric hindrance are highlighted in yellow and each lysine residue is numbered according to its position in the sequence.

Excel sheet S1. Mass, weight loss, and corresponding concentration of solution droplets measured over time during drying.

Excel sheet S2. Proteomic data

Excel sheet S3. Relative amount of amino acids and reactivity: Light chain vs Fibrohexamerin

Video S1. Fluorescent microscopy images of the gradual evaporation of 5μL 2 % RUS (no salts)

Video S2. Fluorescent microscopy images of the gradual evaporation of 5 μL 2 % RUS-KPO.

Supporting references

1. Zaki, M.; Rajkhowa, R.; Holland, C.; Razal, J. M.; Hegh, D. Y.; Allardyce, B. J., Anions, Not Cations, Drive Silk Stability and Self-Assembly: Insights from Regenerated Undegummed Silk. *ACS Biomaterials Science & Engineering* **2025**, *11* (9), 5285–5292.
2. Laity, P. R.; Holland, C., Seeking Solvation: Exploring the Role of Protein Hydration in Silk Gelation. *Molecules* **2022,** *27* (2), 551.